Journal of Materials Chemistry B

TEMPO-CONJUGATED TOBACCO MOSAIC VIRUS AS A MAGNETIC RESONANCE IMAGING CONTRAST AGENT FOR DETECTION OF SUPEROXIDE PRODUCTION IN THE INFLAMED LIVER

Journal:	*Journal of Materials Chemistry B*
Manuscript ID	TB-ART-11-2023-002765.R2
Article Type:	Paper
Date Submitted by the Author:	28-Feb-2024
Complete List of Authors:	Lumata, Jenica; The University of Texas at Dallas, Chemistry and Biochemistry Hagge, Laurel; University of Texas at Dallas, Natural Sciences and Mathematics Gaspar, Miguel; The University of Texas at Dallas, Chemistry and Biochemistry Ikeda, Trashi; The University of Texas at Dallas, Ehrman, Ryanne N.; The University of Texas at Dallas, Chemistry and Biochemistry Chiev, Alyssa; University of Texas at Dallas, Chemistry and Biochemistry Koirala, Shailendra; University of Texas at Dallas, Chemistry and Biochemistry Wijesundara, Yalini H.; University of Texas at Dallas, Chemistry and Biochemistry Darwin, Cary; University of Texas at Dallas, Chemistry and Biochemistry Pena, Salvador; The University of Texas Southwestern Medical Center, Advance Imaging Wen, Xiaodong; UT Southwestern Medical Center, Advanced Imaging Wansapura, Janaka; The University of Texas Southwestern Medical Center, Advance Imaging Nielsen, Steven; University of Texas at Dallas, Chemistry & Biochemistry Kovacs, Zoltan; UT Southwestern Medical Center, Advanced Imaging Lumata, Lloyd; University of Texas at Dallas, Physics Gassensmith, Jeremiah; University of Texas at Dallas, Chemistry and Biochemistry

TEMPO-CONJUGATED TOBACCO MOSAIC VIRUS AS A MAGNETIC RESONANCE IMAGING CONTRAST AGENT FOR DETECTION OF SUPEROXIDE PRODUCTION IN THE INFLAMED LIVER

Jenica L. Lumata[1†], Laurel M. Hagge[1,2†], Miguel A. Gaspar[1], Ikeda Trashi[1], Ryanne N. Ehrman[1], Shailendra Koirala[1], Alyssa C. Chiev[1], Yalini H. Wijesundara[1], Cary B. Darwin[1], Salvador Pena[2], Xiaodong Wen[2], Janaka Wansapura[2], Steven O. Nielsen[1], Zoltan Kovacs[2], Lloyd L. Lumata[2,3], and Jeremiah J. Gassensmith[1,2,4,*]

[1]Department of Chemistry and Biochemistry, The University of Texas at Dallas
[2]Advanced Imaging Research Center, The University of Texas Southwestern Medical Center
[3]Department of Physics, The University of Texas at Dallas
[4]Department of Bioengineering, The University of Texas at Dallas
*Email: gassensmith@utdallas.edu
† Authors contributed equally to this work

Abstract:

Superoxide, an anionic dioxygen molecule, plays a crucial role in redox regulation within the body but is implicated in various pathological conditions when produced excessively. Efforts to develop superoxide detection strategies have led to the exploration of organic-based contrast agents for magnetic resonance imaging (MRI). This study compares the effectiveness of two such agents, nTMV-TEMPO and kTMV-TEMPO, for detecting superoxide in a mouse liver model with lipopolysaccharide (LPS)-induced inflammation. The study demonstrates that kTMV-TEMPO, with a strategically positioned lysine residue for TEMPO attachment, outperforms nTMV-TEMPO as an MRI contrast agent. The enhanced sensitivity of kTMV-TEMPO is attributed to its more exposed TEMPO attachment site, facilitating stronger interactions with water protons and superoxide radicals. EPR kinetics experiments confirm kTMV-TEMPO's faster oxidation and reduction rates, making it a promising sensor for superoxide in inflamed liver tissue. *In vivo* experiments using healthy and LPS-induced inflamed mice reveal that reduced kTMV-TEMPO remains MRI-inactive in healthy mice but becomes MRI-active in inflamed livers. The contrast enhancement in inflamed livers is substantial, validating the potential of kTMV-TEMPO for detecting superoxide *in vivo*. This research underscores the importance of optimizing contrast agents for *in vivo* imaging applications. The enhanced sensitivity and biocompatibility of kTMV-TEMPO make it a promising candidate for further studies in the realm of medical imaging, particularly in the context of monitoring oxidative stress-related diseases.

1 Introduction

Superoxide, $O_2^{\bullet-}$, an anionic dioxygen that falls under the reactive oxygen species (ROS) family, is essential in regulating redox activity within the body.[1, 2] However, excessive production of $O_2^{\bullet-}$ has been associated with inflammatory responses, organ transplant failure, progression of cancer, and the onset of neurodegenerative diseases.[3-5] These associations have spurred efforts to develop strategies to detect superoxide. [6-8] Fluorescence is commonly used for ROS detection owing to the ease with which $O_2^{\bullet-}$ can react with dyes, thereby turning "on" or "off" the fluorescent signal;[9, 10] however, optical imaging methods are limited by poor tissue penetration, making them unsuitable for deep-tissue imaging.[10, 11] On the other hand, MRI is a powerful tool that excels in imaging deep tissues while providing three-dimensional anatomical images.[12] In MRI, the contrast agent plays a crucial role in facilitating signal enhancement. Over the past few decades, the development of "smart" contrast agents for MRI has been an ongoing area of active research for several decades.[13-24] Recent advances, for instance, have shown the ability to report concentrations of metals like Ca^{2+} and Zn^{2+} in deep tissue.[25, 26] These probes are particularly valuable as they provide a minimally invasive approach to real-time analyses of metabolic processes within the body.[16, 27] Organic radical contrast agents (ORCAs) are redox-active, biocompatible, metal-free, and stable nitroxide molecules that have shown the potential to serve as contrast agents to help visualize ROS activity by turning "on or off."[28-30] For instance, the reduced form of TEMPO—the hydroxylamine—is MRI silent but, in the presence of $O_2^{\bullet-}$, can oxidize to its MRI active state (**Scheme 1**).[31, 32] This pattern of reactive

signaling makes nitroxide agents a handy tool in detecting a host of ROS for various oxidative stress-induced disease states.

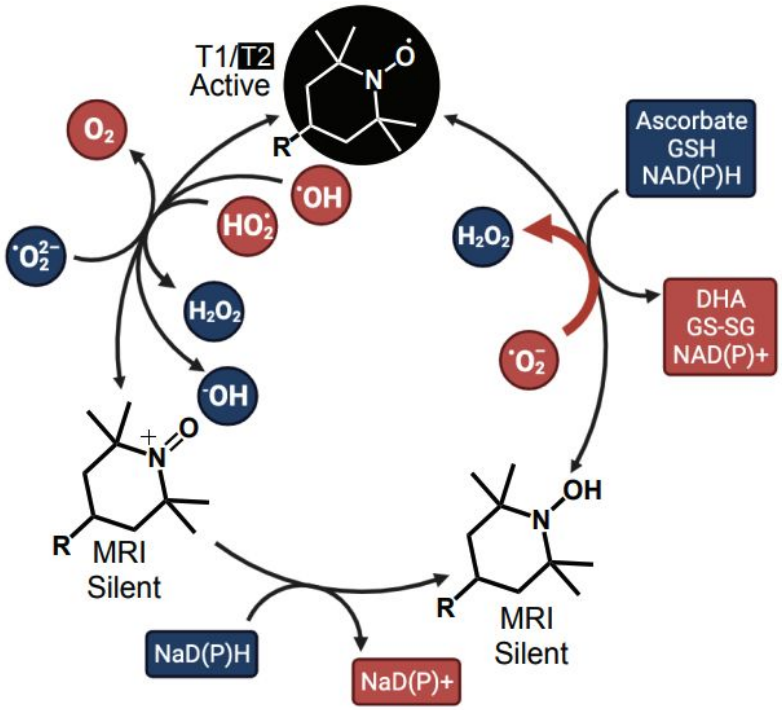

Scheme 1. The redox response of MRI active TEMPO to ROS and reducing agents to form the two "off" species—the oxoammonium (lower left) and the hydroxylamine (lower right) structures.

An issue with exploiting ORCAs like TEMPO as redox-active contrast agents is that they have low relaxivities, which results in weak signal intensity. Studies have demonstrated that enhancing the performance and signal of nitroxide-based superoxide sensors can be achieved by attaching the nitroxide to larger scaffolds.[33-35] Examples of such platforms include nanoparticles[36-38], liposomes[39, 40], micelles[38, 41], polymers[33, 34, 42] and

similar carriers.[43, 44] A previous study from our lab demonstrated the use of a TEMPO-modified tobacco mosaic virus (TMV)[45] contrast agent that could detect superoxide with enhanced T_1 contrast at low field (<3.0 T) and T_2 contrast at high field (9.4 T) with a 4–5 order of magnitude increase in the per-particle T_1 relaxivity (r_1) and T_2 relaxivity (r_2) *in vitro.*[36, 37, 46] The enhancement in relaxivity primarily arises from two key factors. The conjugation of many TEMPO molecules attached to 2130 coat proteins on TMV resulted in high local concentration.[47] Second, TMV's rigid, rod-like structure slows the rotational dynamics in solution, leading to longer rotational correlation times with nearby water molecules, increasing the likelihood of electron-nuclear interactions.[48, 49] These longer interactions of unpaired electrons between the contrast agent and adjacent water protons impact both the T_1 and T_2 relaxation processes.[50, 51] However, this study stopped short of demonstrating redox imaging in a living animal.

In this study, we investigate the efficiency of the redox-active TMV-TEMPO ORCA as an MRI probe in detecting $O_2^{\bullet-}$, a biomarker of liver inflammation. The reduced form—or "off" state—oxidizes in the presence of $O_2^{\bullet-}$, making the probe turn "on", producing a darkening effect in T_2-weighted imaging. To model the oxidative response from a disease state that produces significant ROS, in this work, we monitor the formation of $O_2^{\bullet-}$ induced by lipopolysaccharide (LPS) injected into the liver of female BALB/c rodent models. LPS is an endotoxin that is found on the outer membrane of Gram-negative bacteria.[52] When LPS enters the body, it can trigger a robust immune response, leading to inflammation and superoxide production in the liver and other tissues.[53] LPS is recognized by cells as a natural activator of toll-like receptors (TLRs), especially

TLR4.[54] When LPS binds to TLR4 on immune cells in the liver, it triggers a signaling cascade that activates these cells.[55] This activation includes the production of various pro-inflammatory molecules such as cytokines (*e.g.*, TNF-α, IL-1β, IL-6) and chemokines.[56] These molecules released by activated immune cells signal other cells in the liver and throughout the body to initiate an inflammatory response.[57] Activated immune cells, particularly macrophages, generate $O_2^{\bullet -}$ through a process known as the respiratory burst.[58] The production of superoxide is driven by enzymes such as NADPH oxidase, which transfers electrons from NADPH to molecular oxygen (O_2), producing superoxide.[33, 34]

We previously conducted studies on using wild-type native TMV (nTMV) conjugated to TEMPO (nTMV-TEMPO) as an MRI contrast agent. In this approach, TEMPO is attached to tyrosine (Y139), located on the coat protein's exterior surface. We selected this residue because it provides excellent shielding from reduction, which allows the probe to avoid premature reduction by ascorbate in the blood.[59-61] This approach made nTMV-TEMPO a stable MRI contrast agent but a sluggish sensor for redox processes, making it suboptimal for *in vivo* work. Our research demonstrates that the substitution of a threonine (T) residue with lysine (K) at position 158 (T158K) in a single mutation variant of TMV—denoted as kTMV—results in improved performance of our TEMPO in comparison to the previous attachment of TEMPO to nTMV as illustrated in **Scheme 2A**.[62, 63] kTMV is a well-established site-specific mutant of native TMV; they are effectively identical in tertiary and quaternary structure, but kTMV offers an orthogonal chemical modification site, which we exploit in this work. The versatility of TMV variants

makes them an excellent platform for a wide range of medicinal applications and can provide more ease of chemical modifications, such as the ones in this work. Computational analyses show that the lysine site on kTMV exhibits significantly enhanced solvent exposure (**Figure S2**), facilitating more rapid TEMPO reaction with superoxide radicals. Simultaneously, it allows for efficient trafficking of multiple TEMPO moieties to sites of inflammation, thereby enhancing the MRI signal.

Results and Discussion:

TMV possesses several key attributes that make it particularly well-suited for *in vivo* applications in the realm of medical imaging.[36, 37, 64, 65] First, TMV is noninfectious to humans, eliminating any safety concerns associated with its use.[47, 66] Additionally, TMV exhibits remarkable resilience when exposed to high temperatures, extreme pH conditions, and various chemical manipulations, ensuring its stability during medical procedures.[67, 68] Moreover, TMV demonstrates biocompatibility, making it a viable candidate for integration into biological systems. Structurally, TMV consists of 2130 coat proteins, assembled helically in a 300 nm × 18 nm rod with a pore diameter of 4 nm (**Scheme 2A**). TMV is even more intriguing because its exterior and interior surfaces can be tailored through modifications of solvent-exposed amino acids.[37-40]

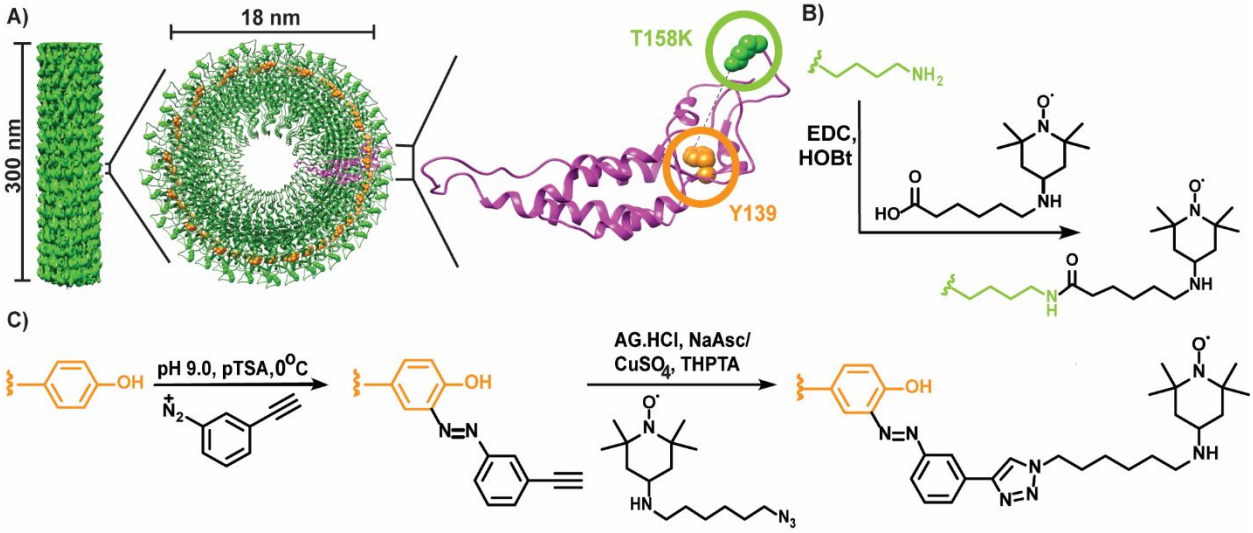

Scheme 2. A) Visual depiction of TMV showing the length of TMV capsid at 300 nm, a diameter of 18 nm, and isolated coat protein. The isolated coat protein shows the T158K mutant and the Y139. The distance between these residues is 24.8 Å. B) Bioconjugation of TEMPO-COOH onto the primary amine of T158K via EDC coupling. C) Bioconjugation of TEMPO-azide on Y139 of nTMV via diazonium coupling followed by copper-azide-alkyne-cycloaddition (CuAAC) to produce nTMV-TEMPO.

Upon closer examination of nTMV from previously discussed literature, it became evident that modification of the kTMV at the T158K position[69] (**Scheme 2B**) would result in a more exposed TEMPO as compared to the modification of nTMV at Y139 (**Scheme 2C**). The Y139 on nTMV is not as prominently exposed on the exterior surface, potentially limiting its ability to interact efficiently with superoxide and water protons, which are crucial for MRI contrast enhancement.[36, 37, 70]

We conducted MD modeling of TMV with nTMV(Y139)-TEMPO and kTMV(T158K)-TEMPO to obtain insight into the dynamics and interactions of these modified proteins. We utilized the 2tmv.pdb structure from the RCSB Protein Data Bank and created a TMV unit cell with either all 49 protein molecules modified at Y139 to incorporate TEMPO (nTMV-TEMPO system) or at T158 to K, further modified to include TEMPO

(kTMV-TEMPO system). These comprehensive models, including the RNA strand, water molecules, and ions, comprised of roughly 312,000 atoms each. Simulations were performed using the NAMD molecular dynamics software for 40 ns, employing the CHARMM all-atom force field and TEMPO parameters from Sezer et al.,[71, 72] supplemented by the CGenFF force field.[73]

The modeling reveals distinct behaviors of TEMPO molecules in the two systems. Both types of TEMPO-modified residues underwent straightening and bending conformational changes, impacting their exposure to water and interaction with other TMV protein residues. However, the kTMV-TEMPO system showed a higher degree of exposure, with the TEMPO radical oxygen atom located more than 1 nm away from the TMV surface 16% of the time, compared to only 2% in the nTMV-TEMPO system (**Figure S1**).

Additionally, we quantified the distribution of electric potentials at the TEMPO radical oxygen atom position, indicating that the kTMV-TEMPO system experiences a broader range of electric potentials, notably including higher values compared to nTMV-TEMPO. This suggests a stronger attraction to negatively charged entities like superoxide and ascorbate for kTMV-TEMPO, although the two systems show similar distributions. Based on these results, the TEMPO in T158K is more likely to extend away from the protein surface significantly and into the solution, along with more favorable electrostatics, which helps explain the faster kinetics of the kTMV-TEMPO system. It also suggests that sensors that detect analytes, especially anionic ones, should not be

placed at the T158K position. On the other hand, to avoid interaction with reactive agents that might destroy the sensor, placing it in the more hidden and stable Y139 position is ideal (**Figure S2**).

Nevertheless, conducting a comparative analysis of these two systems is necessary to explore their respective capabilities as MRI contrast agents in greater detail.

Based on the different residues available from each TMV, TEMPO moieties (**Scheme S1**) were synthesized with different functional arms and characterized through NMR (**Figure S3-5**). Bioconjugations were then performed for each on their respective TMV variant. The TMV-TEMPO variants were characterized with SDS-PAGE, agarose gel, size exclusion chromatography (SEC), and electron paramagnetic resonance (EPR). In **Figure 1A**, SDS-PAGE analysis reveals a band shift for the TMV-TEMPO variants from

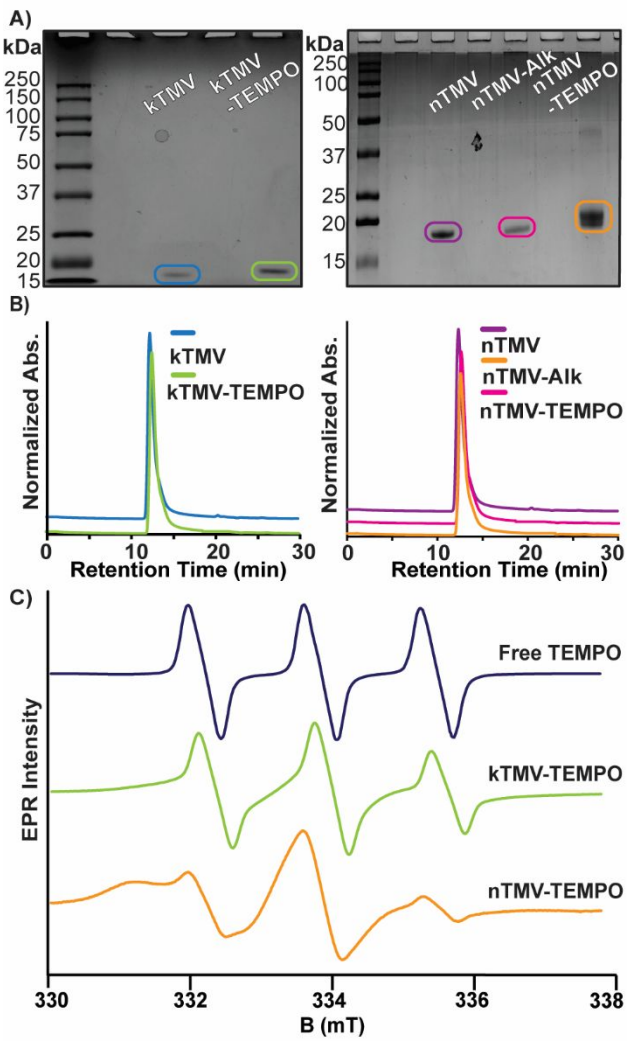

Figure 1. Characterization of nTMV-TEMPO and kTMV-TEMPO. A) 18% SDS-PAGE gels for kTMV-TEMPO and nTMV-TEMPO. B) SEC of kTMV, kTMV-TEMPO, nTMV, nTMV-Alkyne, and nTMV-TEMPO. C) X-band EPR spectra for free TEMPO, kTMV-TEMPO, and nTMV-TEMPO.

the increased molecular weight compared to unmodified TMV. The agarose gel demonstrates a change in migration between unmodified TMV and the modified TMV-TEMPO, indicating the successful TEMPO modification of TMV (**Figure S6**). SEC shows the unchanged size distribution of TMV despite chemical modifications (**Figure 1B**). Since the TMV-TEMPOs are paramagnetic, an EPR experiment was conducted.

Unlike TEMPO, both kTMV-TEMPO and nTMV-TEMPO display asymmetric peaks compared to free TEMPO, suggesting limited mobility due to attachment to the TMV rod (**Figure 1C**).

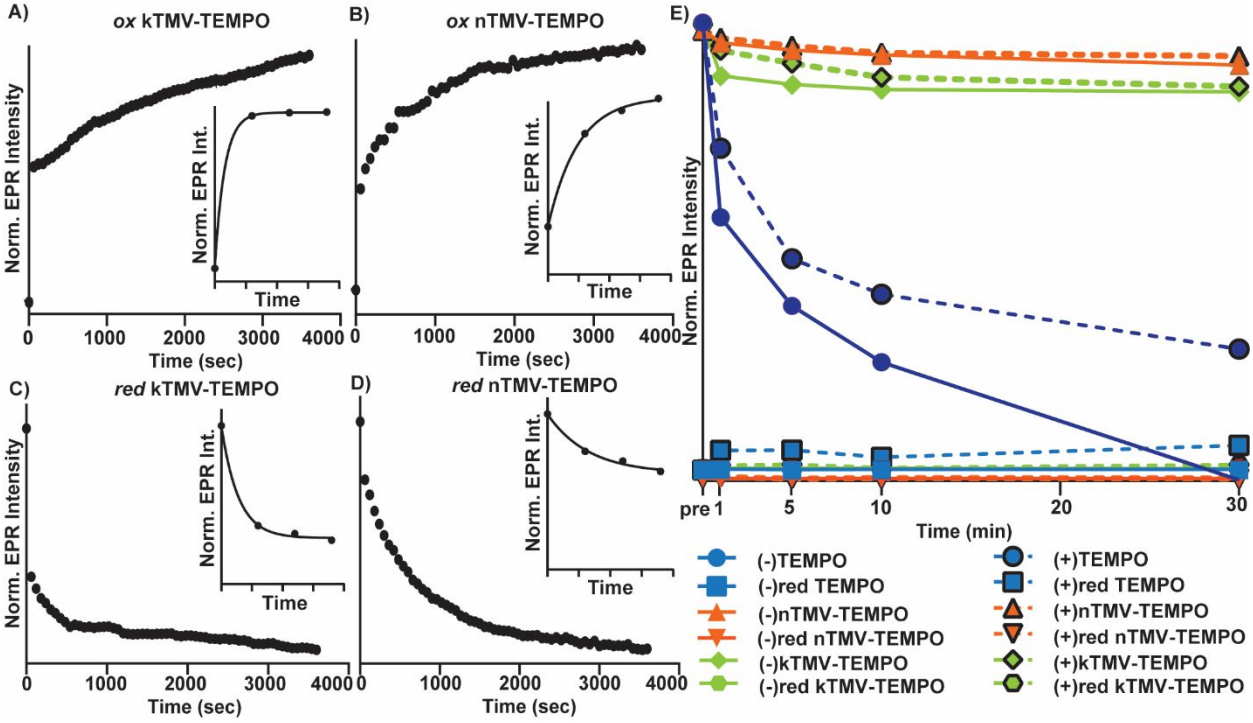

Figure 2. EPR reduction and oxidation fit under pseudo-first order kinetics. The oxidation rate kinetics was conducted by the introduction of potassium superoxide (50 eq) to the reduced TMV-TEMPO variants to monitor the oxidation for 1 h every minute, while for reduction rate, sodium ascorbate (100 eq) was added to TMV-TEMPO variants and were monitored for 1 h. A) Oxidation of reduced kTMV-TEMPO. The first 3 min was magnified for a better view. B) Oxidation of reduced nTMV-TEMPO. C) Reduction of kTMV-TEMPO. D) Reduction of nTMV-TEMPO. E) Redox responses of various agents when exposed to blood from healthy (-) and sick (+) mice via EPR. Data was collected in triplicate but the error bars are not clearly discernible.

To evaluate the speed at which our systems undergo oxidation and reduction, we conducted EPR kinetics experiments (**Figures 2A-D**). One-phase association kinetics were used to measure the rate constants and half-lives ($t_{1/2}$). Both kTMV-TEMPO

(**Figure 2A**) and nTMV-TEMPO (**Figure 2B**) exhibited rapid oxidation kinetics in their reduced states, but it is noteworthy that kTMV-TEMPO demonstrated a notably faster oxidation rate compared to nTMV-TEMPO within the first minute. The EPR signals significantly spiked, covering over half of the total reaction (**Figure 2A and S7**). Because of the rapid initial kinetics, the determination of half-lives and rate constants was split into two segments: the initial 3 minutes and the period following 3 minutes (**Table S1**). Notably, the oxidized kTMV-TEMPO exhibits a shorter $t_{1/2}$ of 11 sec for the first three minutes compared to nTMV-TEMPO ($t_{1/2}$=34 sec), indicating a threefold faster oxidation. This trend is also evident in the reduction rate, with kTMV-TEMPO ($t_{1/2}$=19 sec) reducing approximately twice as rapidly as nTMV-TEMPO ($t_{1/2}$=45 sec). These results further our presupposition that the more exposed TEMPO on kTMV can react more readily with ROS. The swift oxidation rate of reduced kTMV-TEMPO holds promise for its effectiveness as a sensor for superoxide in inflamed liver tissue. The biodistribution of TMV in the blood is known to have a half-life of 10 minutes, with 97% being cleared out in 40 minutes, so our redox rates are within the clearance time of TMV.[63, 74] Finally, these data show that kTMV is indeed more responsive to redox processes compared to nTMV, at least initially, which is important for *in vivo* ROS detection.

MRI agents are injected intravenously in clinical practice so next we considered how blood chemistry would affect the kinetics of the probe. As shown in **Figure 2E**, we investigated the redox responses of different agents when exposed to blood samples obtained from both healthy mice (-) and mice with LPS-induced liver inflammation (+)

using EPR. The agents tested include free TEMPO, nTMV-TEMPO, kTMV-TEMPO, and their respective reduced forms with measurements taken at different time intervals (1 min, 5 min, 10 min, and 30 min). The initial data points represent the EPR signal of the agents in 0.1 M potassium phosphate buffer only. Notably, among the agents, both (-) TEMPO and (+) TEMPO were significantly reduced over a 30 min span. Intriguingly, the relative rates of reduction in the blood depended on the health of the mice, we suspect due to healthy mice having higher concentrations of biological reductants in their system such as ascorbate, saccharides, and cysteine-rich proteins known to impact the reduction kinetics of nitroxides.[75] Mice that had liver inflammation reduced TEMPO less quickly. Presumably, this may be exploitable as an electrochemical sensor for systemic inflammation, possibly as a result of sepsis. The nTMV-TEMPO and kTMV-TEMPO in the blood of both healthy and inflamed mice showed modest reduction over the 30 min. Additionally, the reduced forms displayed no significant changes, except for liver inflamed (+) free TEMPO, which slightly increased at the 1-minute time point.

In preparation for an *in vivo* study, a lactate dehydrogenase (LDH) assay was conducted on RAW 264.7 cells to assess the cytotoxicity of kTMV-TEMPO, nTMV-TEMPO, nTMV, kTMV, and free TEMPO at different concentrations ranging from 0.3125 mg/mL to 10 mg/mL (**Figure S8**). All the tested agents demonstrated a non-cytotoxic profile, with the lowest recorded cell viability remaining at 90% even after a 4 h incubation period. Overall, this further highlights the biocompatibility of TMV-TEMPO variants for *in vivo* applications.

In the context of medical imaging, relaxivity stands as a critical parameter when assessing the effectiveness of contrast agents. It serves as a key indicator of how significantly the variants of TMV-TEMPO elevate the relaxation rate of water molecules within tissue, directly influencing the level of achievable contrast. Put simply, a higher relaxivity value corresponds to a more pronounced enhancement in contrast, making the contrast agent all the more valuable for clinical imaging applications. We measured the relaxivity of TMV-TEMPO variants using a 1T NMR (**Figure 3A**). For free TEMPO, the r_1 value is 0.8715

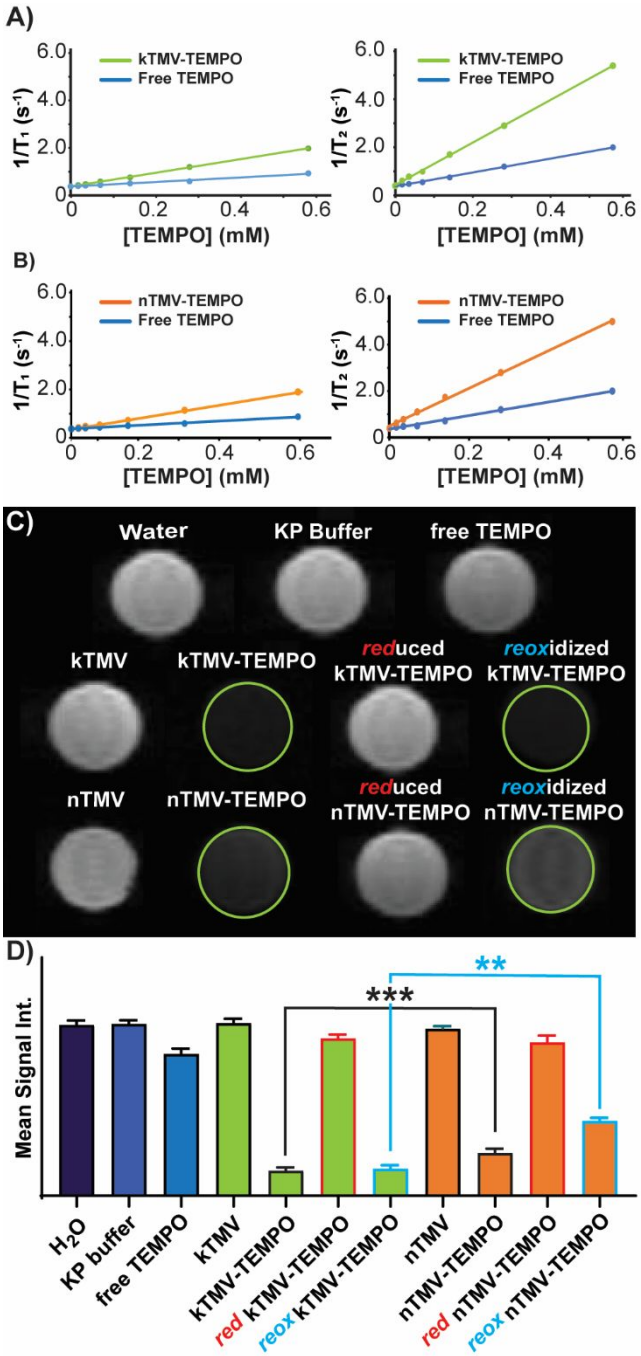

Figure 3. Relaxivity plots of A) kTMV-TEMPO and B) nTMV-TEMPO through T_1- and T_2- weighted scans. C) T_2 weighted MRI of TMV variants, TMV-TEMPO variants, free TEMPO, water, and KP buffer. Both nTMV-TEMPO and kTMV-TEMPO showed the expected T_2 negative contrast. D) Representative plot of T_2 weighted MRI mean signal intensity. Statistical significance was calculated through student t-test [*, $p < 0.05$; **, $p < 0.01$; ***, $p < 0.0005$; ****, $p < 0.0001$; ns = not significant ($p > 0.05$)]

mM^{-1} s^{-1}, and the r_2 value is 2.91 mM^{-1} s^{-1} (**Table S2**). In contrast, nTMV-TEMPO exhibits an r_1 of 2.72 mM^{-1} s^{-1} and an r_2 of 8.11 mM^{-1} s^{-1}, indicating superior T_2 relaxivity. The same is observed in kTMV-TEMPO (r_1 of 2.89 mM^{-1} s^{-1} and an r_2 of 8.97 mM^{-1} s^{-1}). It is also notable that the relaxivity values of kTMV-TEMPO are slightly higher than nTMV-TEMPO. Since the effect of these agents on T_2 is stronger than on T_1, T_2 weighted MRI of phantoms were collected, revealing the expected darkening effect of both kTMV-TEMPO and oxidized nTMV-TEMPO (**Figure 3C**). The results demonstrate that kTMV-TEMPO and oxidized kTMV-TEMPO exhibit a more pronounced T_2 weighted MRI signal (appearing darker or negative contrast) as compared to nTMV-TEMPO and reoxidized nTMV-TEMPO. Notably, the reoxidized kTMV-TEMPO presents a more pronounced negative contrast compared to the reoxidized nTMV-TEMPO, indicating that kTMV-TEMPO displays a higher sensitivity to superoxide. Due to this observation, we opted to move forward with kTMV-TEMPO for further testing in the animal model.

For our *in vivo* analysis, we utilized both normative and pathologically challenged female BALB/c mice, the latter group presenting with liver inflammation induced via direct hepatic injection of LPS eight hours before imaging procedures. T_2 imaging was conducted before and after the administration of contrast agents via caudal (tail) vein injections, capturing both axial and coronal planes at intervals of 5, 10, and 30 minutes post-injection, as depicted in **Figure 4A**. TMV is known to accumulate in the liver, with peak residency appearing at 4 hours, and then is efficiently flushed out of the body over the next 24 hours.[63], [76] First, we administered the oxidized kTMV-TEMPO formulation, which produced a noticeable reduction in signal intensity in the hepatic region within 5

min, as evidenced by the orange outline in **Figure S9**, followed by a gradual normalization of the signal, presumably because the probe was being reduced to its non-MRI active diamagnetic state.

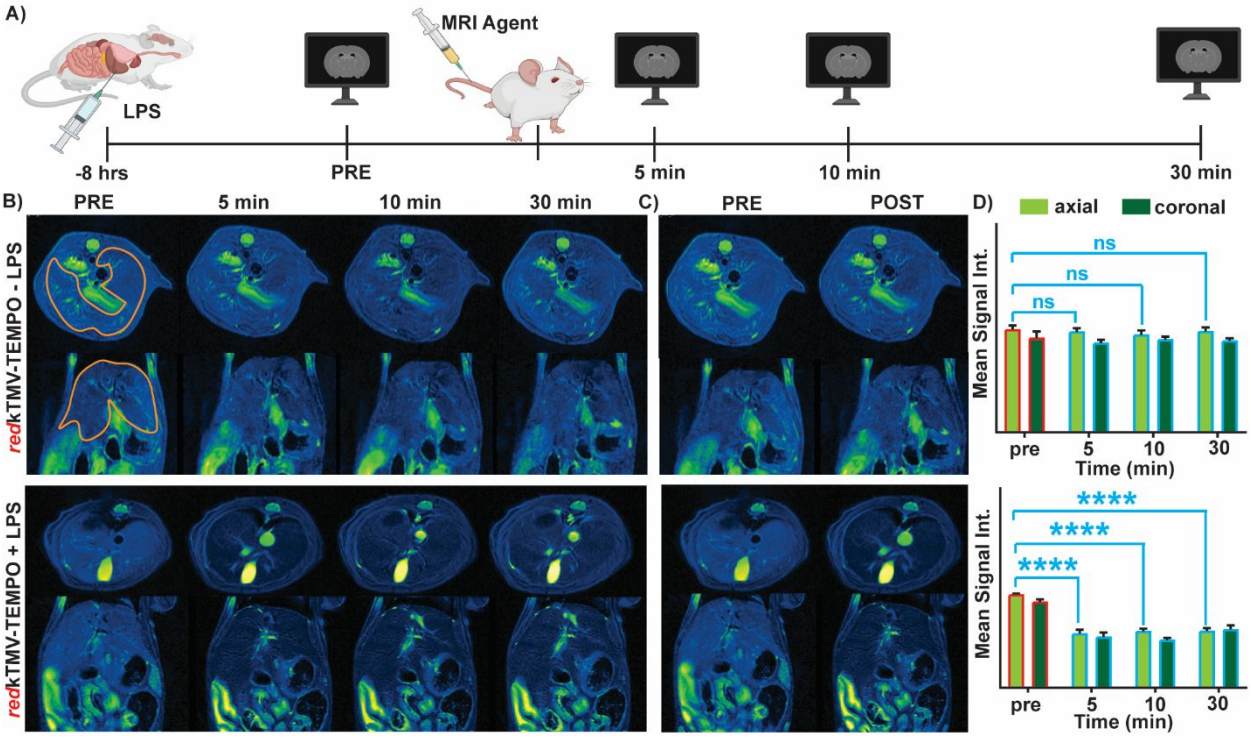

Figure 4. A) Experimental timeline: female BALB/c mice were subjected to liver inflammation through an intrahepatic LPS injection (50 µg/kg) eight hours prior to the initial MRI scan. Following the pre-scan, the mice were administered with reduced kTMV-TEMPO via tail-vein injection, with subsequent scans conducted at 5, 10, and 30 min post-injection. B) T_2- weighted images, oriented on the liver of healthy and sick mice (outlined with an orange line) were administered with reduced kTMV-TEMPO. C) Summarized comparison focusing on the PRE and POST (5 min post-injection) images. D) Mean signal intensity plots at different time points of both healthy and sick mice (N=3). The mice were then positioned in a 3T Bruker MRI scanner. 3D T_2-weighted gradient echo multi-slice scans (TE =48 ms, TR = 1506 ms, Matrix = 128 × 138 × 128). (* $p < 0.05$; **, $p < 0.01$; ***, $p < 0.0005$; ****, $p < 0.0001$; ns = not significant ($p > 0.05$))

Having confirmed that kTMV-TEMPO traffics to the liver, we then conducted a study on the differential response of the non-MRI active reduced kTMV-TEMPO in healthy and inflamed liver tissues. The upper panel of **Figure 4B** demonstrates the application in a

healthy murine model, where the signal intensity before and after injection showed minimal variance, indicating the retention of the MRI-inactive state of reduced kTMV-TEMPO due to the absence of significant levels of $O_2^{\bullet-}$. In stark contrast, the lower panel of **Figure 4B** displays the results of administering reduced kTMV-TEMPO in mice exhibiting liver inflammation. It was observed that the spleen also showed significant darkening in the LPS-injected mice (**Figure S10)**. This is an expected result as the liver and the spleen both play a role in pathogen clearance and metabolism, coined the liver-spleen axis.[77] Here, the post-injection images reveal a marked increase in contrast, suggesting the oxidation of the reduced probe back to its paramagnetic, MRI-active form in response to elevated concentrations of $O_2^{\bullet-}$ in the inflamed tissue. This distinct shift in imaging contrast provides insights into the reactive dynamics of the kTMV-TEMPO agent and underscores its potential as an effective biomarker for *in vivo* detection of oxidative stress and related pathological conditions.

Conclusion

In conclusion, this study provides evidence for the efficacy of kTMV-TEMPO as a redox-active MRI probe for detecting superoxide radicals in inflamed liver tissue, demonstrating its heightened sensitivity and contrast enhancement capabilities. Our findings indicate that the unique structural attributes and dynamics of kTMV-TEMPO, including its increased solvent exposure and efficient interaction with superoxide radicals, significantly enhance its performance as a “smart” MRI contrast agent over nTMV-TEMPO. The use of this ORCA in a living animal model further validates its potential in clinical applications, particularly in the real-time detection and imaging of

oxidative stress-induced pathologies. This work improves upon the previous limitations of concentration dependence by enhancing the MRI properties of the TEMPO through structural enhancement with the mutant TMV. In other words, we obtain significantly greater signal from the same amount of ORCA when placed on the TMV scaffold than the free molecule. With that said, the TMV scaffold does have a relatively fast clearance from the body and this will need to be addressed before clinical application. ORCAs have made significant progress in competing with traditional, lanthanide-based MRI contrast agents, indicating the potential for the emergence of alternative agents. These results underscore the importance of molecular design in developing effective MRI contrast agents and suggest that rational design and careful consideration of structure-function relationships in nanoparticle-based MRI-contrast agents are necessary to optimize their performance, depending on the use case.

Reference

1. H. Sies, V. V. Belousov, N. S. Chandel, M. J. Davies, D. P. Jones, G. E. Mann, M. P. Murphy, M. Yamamoto and C. Winterbourn, *Nature Reviews Molecular Cell Biology*, 2022, **23**, 499-515.
2. G. Pizzino, N. Irrera, M. Cucinotta, G. Pallio, F. Mannino, V. Arcoraci, F. Squadrito, D. Altavilla and A. Bitto, *Oxid Med Cell Longev*, 2017, **2017**, 8416763.
3. E. C. Cheung and K. H. Vousden, *Nature Reviews Cancer*, 2022, **22**, 280-297.
4. R. Varadarajan, L. Golden-Mason, L. Young, P. McLoughlin, N. Nolan, G. McEntee, O. Traynor, J. Geoghegan, J. E. Hegarty and C. O'Farrelly, *Transplantation*, 2004, **78**.
5. B. C. Dickinson and C. J. Chang, *Nature Chemical Biology*, 2011, **7**, 504-511.
6. B. Griffith, S. Pendyala, L. Hecker, P. J. Lee, V. Natarajan and V. J. Thannickal, *Antioxidants & Redox Signaling*, 2009, **11**, 2505-2516.
7. S. Missiroli, I. Genovese, M. Perrone, B. Vezzani, V. A. M. Vitto and C. Giorgi, *Journal*, 2020, **9**.
8. M. A. Venkatachalam, K. A. Griffin, R. Lan, H. Geng, P. Saikumar and A. K. Bidani, *American Journal of Physiology-Renal Physiology*, 2010, **298**, F1078-F1094.
9. Y. Zhang, J. Parrondo, S. Sankarasubramanian and V. Ramani, *ChemSusChem*, 2017, **10**, 3056-3062.

10. C. C. Winterbourn, *Biochimica et Biophysica Acta (BBA) - General Subjects*, 2014, **1840**, 730-738.
11. B. Kalyanaraman, V. Darley-Usmar, K. J. A. Davies, P. A. Dennery, H. J. Forman, M. B. Grisham, G. E. Mann, K. Moore, L. J. Roberts and H. Ischiropoulos, *Free Radical Biology and Medicine*, 2012, **52**, 1-6.
12. J. L. Nelissen, W. A. Traa, H. H. de Boer, L. de Graaf, V. Mazzoli, C. D. Savci-Heijink, K. Nicolay, M. Froeling, D. L. Bader, A. J. Nederveen, C. W. J. Oomens and G. J. Strijkers, *Journal of Applied Physiology*, 2018, **124**, 1580-1596.
13. H. Li and T. J. Meade, *Journal of the American Chemical Society*, 2019, **141**, 17025-17041.
14. J. L. Major and T. J. Meade, *Accounts of Chemical Research*, 2009, **42**, 893-903.
15. V. Nandwana, M. De, S. Chu, M. Jaiswal, M. Rotz, T. J. Meade and V. P. Dravid, in *Nanotechnology-Based Precision Tools for the Detection and Treatment of Cancer*, eds. C. A. Mirkin, T. J. Meade, S. H. Petrosko and A. H. Stegh, Springer International Publishing, Cham, 2015, DOI: 10.1007/978-3-319-16555-4_3, pp. 51-83.
16. L. M. De Leon-Rodriguez, A. J. M. Lubag, C. R. Malloy, G. V. Martinez, R. J. Gillies and A. D. Sherry, *Accounts of Chemical Research*, 2009, **42**, 948-957.
17. J. Lux and A. D. Sherry, *Current Opinion in Chemical Biology*, 2018, **45**, 121-130.
18. L. M. Hagge, A. Shahrivarkevishahi, N. M. Al-Kharji, Z. Chen, O. R. Brohlin, I. Trashi, A. Tumac, F. C. Herbert, A. V. Adlooru, H. Lee, H. R. Firouzi, S. A. Cornelius, N. J. De Nisco and J. J. Gassensmith, *Journal of Materials Chemistry B*, 2023, **11**, 7126-7133.
19. I. Trashi, M. Z. Durbacz, O. Trashi, Y. H. Wijesundara, R. N. Ehrman, A. C. Chiev, C. B. Darwin, F. C. Herbert, J. Gadhvi, N. J. De Nisco, S. O. Nielsen and J. J. Gassensmith, *Journal of Materials Chemistry B*, 2023, **11**, 4445-4452.
20. P. Parsamian, Y. Liu, C. Xie, Z. Chen, P. Kang, Y. H. Wijesundara, N. M. Al-Kharji, R. N. Ehrman, O. Trashi, J. Randrianalisoa, X. Zhu, M. D'Souza, L. A. Wilson, M. J. Kim, Z. Qin and J. J. Gassensmith, *ACS Nano*, 2023, **17**, 7797-7805.
21. A. Shahrivarkevishahi, M. A. Luzuriaga, F. C. Herbert, A. C. Tumac, O. R. Brohlin, Y. H. Wijesundara, A. V. Adlooru, C. Benjamin, H. Lee, P. Parsamian, J. Gadhvi, N. J. De Nisco and J. J. Gassensmith, *Journal of the American Chemical Society*, 2021, **143**, 16428-16438.
22. F. C. Herbert, O. R. Brohlin, T. Galbraith, C. Benjamin, C. A. Reyes, M. A. Luzuriaga, A. Shahrivarkevishahi and J. J. Gassensmith, *Bioconjugate Chemistry*, 2020, **31**, 1529-1536.
23. C. E. Benjamin, Z. Chen, P. Kang, B. A. Wilson, N. Li, S. O. Nielsen, Z. Qin and J. J. Gassensmith, *Journal of the American Chemical Society*, 2018, **140**, 17226-17233.
24. H. Lee, C. E. Benjamin, C. M. Nowak, L. H. Tuong, R. P. Welch, Z. Chen, M. Dharmarwardana, K. W. Murray, L. Bleris, S. D'Arcy and J. J. Gassensmith, *Molecular Pharmaceutics*, 2018, **15**, 2984-2990.
25. G. Wang and G. Angelovski, *Angewandte Chemie International Edition*, 2021, **60**, 5734-5738.
26. A. Barandov, B. B. Bartelle, C. G. Williamson, E. S. Loucks, S. J. Lippard and A. Jasanoff, *Nature Communications*, 2019, **10**, 897.
27. Q. N. Do, J. S. Ratnakar, Z. Kovács and A. D. Sherry, *ChemMedChem*, 2014, **9**, 1116-1129.

28. F. Hyodo, K.-H. Chuang, A. G. Goloshevsky, A. Sulima, G. L. Griffiths, J. B. Mitchell, A. P. Koretsky and M. C. Krishna, *Journal of Cerebral Blood Flow & Metabolism*, 2008, **28**, 1165-1174.
29. F. Hyodo, K.-i. Matsumoto, A. Matsumoto, J. B. Mitchell and M. C. Krishna, *Cancer Research*, 2006, **66**, 9921-9928.
30. K.-i. Matsumoto, I. Nakanishi, Z. Zhelev, R. Bakalova and I. Aoki, *Antioxidants & Redox Signaling*, 2021, **36**, 95-121.
31. Z. Zhelev, E. Georgieva, D. Lazarova, S. Semkova, I. Aoki, M. Gulubova, T. Higashi and R. Bakalova, *Oxidative Medicine and Cellular Longevity*, 2019, **2019**, 6373685.
32. S. A. Shah, S. X. Cui, C. D. Waters, S. Sano, Y. Wang, H. Doviak, J. Leor, K. Walsh, B. A. French and F. H. Epstein, *NMR in Biomedicine*, 2020, **33**, e4359.
33. M. A. Sowers, J. R. McCombs, Y. Wang, J. T. Paletta, S. W. Morton, E. C. Dreaden, M. D. Boska, M. F. Ottaviani, P. T. Hammond, A. Rajca and J. A. Johnson, *Nature Communications*, 2014, **5**, 5460.
34. H. V. T. Nguyen, Q. Chen, J. T. Paletta, P. Harvey, Y. Jiang, H. Zhang, M. D. Boska, M. F. Ottaviani, A. Jasanoff, A. Rajca and J. A. Johnson, *ACS Central Science*, 2017, **3**, 800-811.
35. G. G. Alvaradejo, H. V. T. Nguyen, P. Harvey, N. M. Gallagher, D. Le, M. F. Ottaviani, A. Jasanoff, G. Delaittre and J. A. Johnson, *ACS Macro Letters*, 2019, **8**, 473-478.
36. H. Lee, A. Shahrivarkevishahi, J. L. Lumata, M. A. Luzuriaga, L. M. Hagge, C. E. Benjamin, O. R. Brohlin, C. R. Parish, H. R. Firouzi, S. O. Nielsen, L. L. Lumata and J. J. Gassensmith, *Chemical Science*, 2020, **11**, 2045-2050.
37. M. Dharmarwardana, A. F. Martins, Z. Chen, P. M. Palacios, C. M. Nowak, R. P. Welch, S. Li, M. A. Luzuriaga, L. Bleris, B. S. Pierce, A. D. Sherry and J. J. Gassensmith, *Molecular Pharmaceutics*, 2018, **15**, 2973-2983.
38. S. Guo, X. Wang, Z. Li, D. Pan, Y. Dai, Y. Ye, X. Tian, Z. Gu, Q. Gong, H. Zhang and K. Luo, *Journal of Nanobiotechnology*, 2021, **19**, 244.
39. C. Liu, K. K. Ewert, N. Wang, Y. Li, C. R. Safinya and W. Qiao, *Biomaterials*, 2019, **221**, 119412.
40. D. Alberti, E. Thiaudiere, E. Parzy, S. Elkhanoufi, S. Rakhshan, R. Stefania, P. Massot, P. Mellet, S. Aime and S. Geninatti Crich, *Scientific Reports*, 2023, **13**, 13725.
41. K. Nagura, A. Bogdanov, N. Chumakova, A. K. Vorobiev, S. Moronaga, H. Imai, T. Matsuda, Y. Noda, T. Maeda, S. Koizumi, K. Sakamoto, T. Amano, F. Yoshino, T. Kato, N. Komatsu and R. Tamura, *Nanotechnology*, 2019, **30**, 224002.
42. H. V. T. Nguyen, A. Detappe, N. M. Gallagher, H. Zhang, P. Harvey, C. Yan, C. Mathieu, M. R. Golder, Y. Jiang, M. F. Ottaviani, A. Jasanoff, A. Rajca, I. Ghobrial, P. P. Ghoroghchian and J. A. Johnson, *ACS Nano*, 2018, **12**, 11343-11354.
43. Y. H. Chung, H. Cai and N. F. Steinmetz, *Advanced Drug Delivery Reviews*, 2020, **156**, 214-235.
44. K.-A. Hansen and J. P. Blinco, *Polymer Chemistry*, 2018, **9**, 1479-1516.
45. J. N. Culver, *Annual Review of Phytopathology*, 2002, **40**, 287-308.
46. X. Mao, J. Xu and H. Cui, *WIREs Nanomedicine and Nanobiotechnology*, 2016, **8**, 814-841.

47. J. L. Lumata, D. Ball, A. Shahrivarkevishahi, M. A. Luzuriaga, F. C. Herbert, O. Brohlin, H. Lee, L. M. Hagge, S. D'Arcy and J. J. Gassensmith, *Scientific Reports*, 2021, **11**, 15109.
48. L. Liepold, S. Anderson, D. Willits, L. Oltrogge, J. A. Frank, T. Douglas and M. Young, *Magnetic Resonance in Medicine*, 2007, **58**, 871-879.
49. S. Qazi, L. O. Liepold, M. J. Abedin, B. Johnson, P. Prevelige, J. A. Frank and T. Douglas, *Molecular Pharmaceutics*, 2013, **10**, 11-17.
50. A. D. Sherry and Y. Wu, *Current Opinion in Chemical Biology*, 2013, **17**, 167-174.
51. J. Wahsner, E. M. Gale, A. Rodríguez-Rodríguez and P. Caravan, *Chemical Reviews*, 2019, **119**, 957-1057.
52. M. Matsuura, *Frontiers in Immunology*, 2013, **4**, 109.
53. D. Heumann and T. Roger, *Clinica Chimica Acta*, 2002, **323**, 59-72.
54. A. Zamyatina and H. Heine, *Frontiers in Immunology*, 2020, **11**.
55. J.-B. Soares, P. Pimentel-Nunes, R. Roncon-Albuquerque and A. Leite-Moreira, *Hepatology International*, 2010, **4**, 659-672.
56. E. Seki, H. Tsutsui, H. Nakano, N. M. Tsuji, K. Hoshino, O. Adachi, K. Adachi, S. Futatsugi, K. Kuida, O. Takeuchi, H. Okamura, J. Fujimoto, S. Akira and K. Nakanishi, *The Journal of Immunology*, 2001, **166**, 2651-2657.
57. L. Chen, H. Deng, H. Cui, J. Fang, Z. Zuo, J. Deng, Y. Li, X. Wang and L. Zhao, *Oncotarget; Vol 9, No 6*, 2017.
58. K. E. Iles, Forman, H.J., *Immunol Res*, 2002, **26**, 95-105.
59. L. Injarabian, M. Scherlinger, A. Devin, S. Ransac, J. Lykkesfeldt and B. S. Marteyn, *Scientific Reports*, 2020, **10**, 10659.
60. B. Frei, L. England and B. N. Ames, *Proceedings of the National Academy of Sciences of the United States of America*, 1989, **86**, 6377-6381.
61. M. Przybyło and M. Langner, *Cellular & Molecular Biology Letters*, 2020, **25**, 32.
62. E. F. J. Geiger F C, Eiben S, Mueller A, Jeske H, Spatz J P, Wege C, *Nanoscale*, 2013, **5**, 3808-3816.
63. H. H. A. S. Pitek, S. Shukla, N.F. Steinmetz, *ACS Appl. Mater. Interfaces*, 2018, **10**, 39468-39477.
64. M. A. Bruckman, K. Jiang, E. J. Simpson, L. N. Randolph, L. G. Luyt, X. Yu and N. F. Steinmetz, *Nano Letters*, 2014, **14**, 1551-1558.
65. M. A. Bruckman, S. Hern, K. Jiang, C. A. Flask, X. Yu and N. F. Steinmetz, *Journal of Materials Chemistry B*, 2013, **1**, 1482-1490.
66. S. Li and J. J. Gassensmith, in *Protein Scaffolds: Design, Synthesis, and Applications*, ed. A. K. Udit, Springer New York, New York, NY, 2018, DOI: 10.1007/978-1-4939-7893-9_8, pp. 95-108.
67. M. A. Luzuriaga, R. P. Welch, M. Dharmarwardana, C. E. Benjamin, S. Li, A. Shahrivarkevishahi, S. Popal, L. H. Tuong, C. T. Creswell and J. J. Gassensmith, *ACS Applied Materials & Interfaces*, 2019, **11**, 9740-9746.
68. S. Li, M. Dharmarwardana, R. P. Welch, C. E. Benjamin, A. M. Shamir, S. O. Nielsen and J. J. Gassensmith, *ACS Applied Materials & Interfaces*, 2018, **10**, 18161-18169.
69. F. C. Geiger, F. J. Eber, S. Eiben, A. Mueller, H. Jeske, J. P. Spatz and C. Wege, *Nanoscale*, 2013, **5**, 3808-3816.

70. Z. Chen, N. Li, S. Li, M. Dharmarwardana, A. Schlimme and J. J. Gassensmith, *WIREs Nanomedicine and Nanobiotechnology*, 2016, **8**, 512-534.
71. D. Sezer, J. H. Freed and B. Roux, *The Journal of Physical Chemistry B*, 2008, **112**, 5755-5767.
72. K. Vanommeslaeghe, E. P. Raman and A. D. MacKerell, Jr., *Journal of Chemical Information and Modeling*, 2012, **52**, 3155-3168.
73. K. Vanommeslaeghe and A. D. MacKerell, Jr., *Journal of Chemical Information and Modeling*, 2012, **52**, 3144-3154.
74. J. S. Man Wu, Di Fan, Quan Zhou, Fan Wang, Zhongwei Niu, and Yong Huang *Biomacromolecules* 2013, **14**, 4032-4037.
75. s
76. L. N. R. Michael A. Bruckman, Allen VanMeter, Stephen Hern, Andrew J. Shoffstall, Rebecca E. Taurog, Nicole F. Steinmetz, *Virology*, 2014, **449**, 163-173.
77. S. A. Tarantino G, Finelli C., *World J Gastroenterol.*, 2013, **19**, 3534-3542.